Journal of Industrial and Engineering Chemistry 54 (2017) 341–349

Contents lists available at ScienceDirect

Journal of Industrial and Engineering Chemistry

journal homepage: www.elsevier.com/locate/jiec

Green strategy to produce large core–shell affinity beads for gravity-driven API purification processes

Raquel Viveiros[a,b], Francisco M. Dias[c], Luisa B. Maia[d], William Heggie[b], Teresa Casimiro[a,*]

[a] LAQV–REQUIMTE, Departamento de Química, Faculdade de Ciências e Tecnologia, Universidade NOVA de Lisboa, 2829-516 Caparica, Portugal
[b] Hovione FarmaCiencia SA, R&D, Sete Casas, 2674-506 Loures, Portugal
[c] Instituto de Plasmas e Fusão Nuclear, Instituto Superior Técnico, Universidade de Lisboa, 1049-001, Portugal
[d] UCIBIO–REQUIMTE, Departamento de Química, Faculdade de Ciências e Tecnologia, Universidade NOVA de Lisboa, 2829-516 Caparica, Portugal

ARTICLE INFO

Article history:
Received 3 February 2017
Received in revised form 6 April 2017
Accepted 5 June 2017
Available online 15 June 2017

Keywords:
Supercritical carbon dioxide
3-(Trimethoxysilyl) propyl methacrylate
Plasma technology functionalization
Genotoxin removal
Surface imprinting technique

ABSTRACT

In this work, Molecular Imprinted Polymers (MIPs)-layered silica beads which have affinity for a model pharmaceutical impurity, acetamide (ACET) were developed using supercritical carbon dioxide ($scCO_2$) technology. Silica beads were first functionalized using two different green strategies, *grafting to* (MPS/EtOH in $scCO_2$) and *grafting from* (plasma technology). These core beads were then used as seed particles in the synthesis, in $scCO_2$ of a MIP layer. Dynamic binding tests were performed in order to evaluate the affinity of the resulting silica core – MIP shell beads to ACET and the efficiency of its removal from an active pharmaceutical ingredient – Beclomomethasone dipropionate (API) crude mixture. ACET was preferentially retained over analogue molecules, benzamide (BENZ) and pivalamide (PIV). The core–shell MIP beads were packed in a SPE column (396.5 mg in a 3 mL SPE tube) and evaluated as a potential gravity-driven purification device, enabling the removal of 100% of ACET whilst losing only 0.37% of API from a model mixture solution—10 mL of ACET and API (0.25 mg mL^{-1} + 3.5 mg mL^{-1}).

Introduction

Purification of APIs is a paramount issue in the pharmaceutical industry. During API manufacturing, reactive intermediates (catalysts, acids, inorganic salts, etc.), among others are often obtained at trace levels in the final drug product. Genotoxins are a particular class of pharmaceutical impurities which have gained a great deal of attention by pharmaceutical regulatory agencies since they have the ability to interact with DNA causing gene mutations [1]. Reflecting the general concern regarding the role of chemicals and their impact on human health and environment, the (EMEA) issued strict limits for genotoxins in pharmaceutical products [2]. FDA has also developed a metric to define the level of exposure to a genotoxic impurity that is considered to represent a negligible risk to human health. The limit of 1.5 μg/day—the threshold of toxicological concern (TTC) was set for an average adult weighing 70 kg [3]. These limits for genotoxins in APIs have forced the Pharmaceutical Industry to develop strategies which are able to reduce the genotoxin content to below the specified values whilst containing costs at acceptable levels.

Multi-step processes such as distillation, adsorption–desorption, solvent extraction, fractional crystallization and chromatography are some of well-known processes commonly used in API purification but unfortunately, are time-consuming, involve expensive steps or a high percentage of API loss, which all contribute to an increase in the cost of the final product [4,5,6]. Hence, a major challenge facing the Pharmaceutical Industry is to design processes which minimize the formation of impurities and to elaborate efficient strategies to remove genotoxin residues efficiently.

Herein, we will focus on a specific genotoxin, acetamide (ACET), which can arise in pharmaceutical manufacturing and has potential carcinogenic behavior. The admissible TTC limit for ACET is at the ppm level [7].

In recent years, fresh approaches have been described for API manufacturing processes such as quality by design and redesign of the API synthetic strategies to avoid impurities [8,9]. In addition, new purification processes such as molecularly imprinted polymers (MIPs) as solid-phase adsorbents, MIP-based membranes, nanofiltration or the combination of these methodologies have been proposed [10,11].

* Corresponding author. Fax: +351 212 948 550.
E-mail address: teresa.casimiro@fct.unl.pt (T. Casimiro).

http://dx.doi.org/10.1016/j.jiec.2017.06.012
1226-086X/

MIPs take advantage of the fact that they have a high affinity for the template molecule and thus have a huge potential for these applications due to their high structural selectivity. Unfortunately, in general, polymers have slow mass transfer and inaccessible binding sites located deep inside the bulk of the polymer matrix [12,13]. MIP particles for solid-phase extraction (SPE) have been used with particle size diameters between 25 and 60 μm [14] which correspond to a small fraction of the polymer produced leading to a lot of waste. In addition, the use of these particles in SPE necessarily involves the use of applied pressure or vacuum. In order to increase the accessibility to molecular imprinted sites, several kinds of particles have been developed (e.g. silica, titanium oxide aluminum, poly(styrene-co-divinylbenzene), etc) with regular and irregular forms and with sizes from 400 nm to 150 μm, containing MIPs at the particle's surface [15,16]. A desirable objective is consequently to produce particles with a diameter greater than 75 μm and with regular morphology thus, allowing them to be packed into gravity-driven columns resulting in a cheaper and more easily operated separation process.

In addition, a surface imprinting technique overcomes the low mass-transfer drawback by locating the sites at the surface or in the proximity of the surface, enabling good accessibility during the final application [17,18]. Advantages are high MIP surface-to-particle volume ratio, good dispersion, rapid binding kinetics [19] and the template within the thin shells can be completely removed to form effective recognition sites [20]. In addition, properties of the final particles such as size, functionality and thickness can be controlled [21]. This methodology can easily be applied to the facile preparation of polymer-grafted silica.

Physisorption [22,23],*grafting to* and *grafting from* are the most cited methods to functionalize or activated surfaces for preparation of surface imprinted polymers [12,24]. Here, we focus on *grafting to* and *grafting from* as strategies to graft polymer chains at the surface of the core–shell beads. The "*grafting to*" method involves a chemical reaction to functionalize the support. The polymerization process occurs in the presence of this pre-functionalized support with functional groups at its surface, an initiator being required to promote the growth of the polymer chains. On the other hand, in the "*grafting from*" method an initiator is previously anchored at the surface and the polymerization process occurs in the presence of surface-attached initiator followed by *in situ* polymerization [25]. This method can be performed by combining plasma surface activation and in situ supercritical fluid-assisted polymerization [26].

Supercritical carbon dioxide ($scCO_2$) is an alternative green solvent which has already proved to be an excellent medium to produce and process polymers with controlled properties. Moreover, MIPs have been produced in $scCO_2$ for several different applications [27–29].

Stojanovic et al. reported the production of nanoparticles of silica with a polymer layer of PMMA in $scCO_2$ [30,31]. There are also reported methods to form polymer coatings/encapsulation of nanoparticles using supercritical anti-solvent processes, but these have no applicability to gravity-driven processes. MIP-silica gel particles (210–500 μm) to be used in gravity chromatography columns were also reported by Prasad et al. to enrich β-lactam antibiotics [32] and a diquat herbicide [33] wherein the MIP layer was produced by conventional methods.

In this work we report for the first time the production of MIP core–shell beads in $scCO_2$ with particle size ranging from 75 to 200 μm, which is a suitable size for gravity-driven purification processes. A shell of MIP was produced on top of a silica core for use in the selective removal of ACET from crude mixtures of the API, Beclomomethasone dipropionate. The work comprises: (1) functionalization of the core beads with *grafting to* and *grafting from* approaches using green technologies and; (2) production of a MIP-layer over the core in $scCO_2$ wherein the core-support, functional monomer (MAA), cross-linker (EGDMA) and template molecule (ACET) are all present.

The core–shell MIP beads were obtained ready to be packed into SPE devices, which were further evaluated using a model pharmaceutical mixture containing ACET and API respectively. Beclomethasone dipropionate [34] is a potent glucocorticoid steroid used in treatment of asthma [35] and rhinitis [36].

Experimental

Materials

Acetamide (ACET, 99% purity) as template (Fig. 1), benzamide (BENZ, 99% purity) and trimethylacetamide (Pivalamide, PIV, 98% purity) as analogue molecules, methacrylic acid (MAA, 99% purity) as functional monomer, ethylene glycol dimethacrylate (EGDMA, 98% purity) as cross-linker, silica gel 75–200 μm (mean pore size 110 Å and surface area 250–350 $m^2 g^{-1}$) and 3-(Trimethoxysilyl) propyl methacrylate (MPS, 98% purity) as silane coupling agent were purchased from Sigma-Aldrich. Azobis(isobutyronitrile) (AIBN, 98% purity) from Fluka was used as initiator. Beclomethasone dipropionate (Fig. 1) was kindly provided by Hovione FarmaCiencia SA (Portugal). Ethanol absolute analytical grade from Scharlau and HPLC grade acetonitrile (ACN) from Carlo Erba were used. SPE syringes Supelclean TM LC-Ph SPE Tubes 3 mL were purchased from Supelco. Carbon dioxide was obtained from Air Liquide with purity greater than 99.998%. All chemicals were used without further purification.

Functionalization of silica core particles

Grafting to— MPS/EtOH-$scCO_2$ surface functionalization

Surface modification of silica beads was performed in a 33 mL stainless steel high-pressure cell equipped with two aligned sapphire windows. Silica particles (0.50 g) were mixed with ethanol (10% v/v) under magnetic stirring for 15 min and ultrasonically treated for 30 min at room temperature. In the next step, 4.78 mL of MPS coupling agent was added dropwise to the silica. The high-pressure vessel was then sealed, and CO_2 pumped into the system. When the desired pressure and temperature were attained (40 °C, 20 MPa), stirring was initiated. At the end of the process, the outlet valve was opened, thereby providing a constant flow of CO_2 for 2 h and a clean-up of the modified particles. These particles were finally dried at room temperature under vacuum for 4 h and then dried in an oven under atmospheric pressure at 110 °C for a further 2 h [31], yielding the MPS-modified silica particles.

Grafting from—Plasma functionalization of silica core beads

Silica particles were functionalized by microwave plasma under low pressure conditions. 1 g of silica was used in each experiment. Silica particles were functionalized using two different conditions: **E1** (Flow: 50 sccm argon; Time: 20 min) and **E2** (Flow: 47.5 sccm

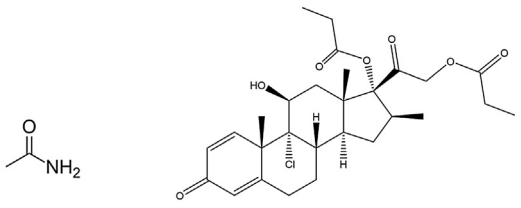

Acetamide (**ACET**) Beclomethasone dipropionate (**API**)

Fig. 1. Structures of acetamide (ACET) and beclomethasone dipropionate (API).

argon and 2.5 sccm H_2; Time: 20 min). The experiments were performed using large-scale, slot-antenna excited microwave plasmas driven by surface waves [37]. The antennas (slots in a rectangular waveguide) are separated from the discharge vessel by a quartz plate. The microwave power is provided by a 2.45 GHz generator (Sairem), whose output power was kept constant at 600 W. A 3-stub matching device and a variable short-circuit ensure a negligible value for the reflected power. The discharge takes place inside a water-cooled aluminum block, whose internal diameter and length are 22 and 10 cm, respectively, and diffuses into 30 cm in diameter pyrex chamber, where the microwave field is virtually "zero". A lateral port enables a convenient access to the pyrex chamber for the insertion and removal of samples. Samples are treated laying on top of a fused silica dish attached to an axially movable piston, which enables adjusting the position of samples relatively to the active discharge zone hence to control local values of plasma parameters [38]. Treatments were carried out at 7 cm from the quartz plate mentioned earlier. During the treatment, the pressure remained constant at 1.0 mbar, corresponding to a total gas flow of 50 sccm for the pumping system used. At the end of the run the plasma chamber was ventilated and the functionalized particles collected and stored in an inert atmosphere until their use.

Synthesis of large core–shell imprinted beads

Batch polymerization reactions at the silica surface were carried out in $scCO_2$. The polymerization is similar to that reported in the literature [39]. In a typical experiment to produce the core–shell MIP beads, 0.5 g of pre-functionalized silica, by the methods described above (*grafting to* and *grafting from*), 1 mmol of the template molecule ACET, 4 mmol of the functional monomer MAA, 20 mmol of the cross-linker agent EGDMA and 1 wt% of the radical initiator AIBN (only in silica functionalized using the *grafting to* method) were introduced into a 33 mL stainless steel high-pressure cell equipped with two aligned sapphire windows and a Teflon® coated magnetic stirrer bar. The cell was immersed in a thermostatic water bath at 65 °C, the optimal AIBN initiation temperature. Temperature control was achieved through an open bath circulator Julabo Ed with stability ± 0.1 °C. Carbon dioxide was added up to 21 MPa and the polymerization reactions allowed to proceeded for 24 h under stirring. At these initial temperature and pressure conditions, with exception of the core beads, all reactants were completely dissolved in the supercritical phase. At the end of the reaction, the core–shell MIP beads were slowly washed with fresh supercritical CO_2 for 1 h in order to remove the template molecule and wash out any unreacted residues. Si-MPS-MIPs refers to the *grafting to* method, while Si-Plasma-E1-MIPs and Si-Plasma-E2-MIPs are samples from *grafting from* method. Core–shell NIP beads were synthesized following the same procedure without addition of template.

Template desorption from core–shell MIP beads using $scCO_2$ technology

$scCO_2$-assisted ACET desorption was performed using a continuous extraction process. For that, core–shell MIP beads were loaded and compacted in a tubular reactor coupled with a 33 mL stainless steel high-pressure cell with 3 mL of ACN and CO_2 until 21 MPa was reached. Two high pressure cells were immersed in a thermostatic water bath at 40 °C for 3 h with a continuous flux in order to remove all the template from the matrix.

Characterization methods

SEM analysis was performed on a Hitachi S-2400 instrument, with an accelerating voltage set to 15 kV. Samples were mounted on aluminum stubs using carbon tape and were gold coated. Specific surface area and pore diameter of polymer powders were determined by N_2 adsorption according to the BET method. Nitrogen sorption porosimetry measurements were performed on an ASAP 2010 Accelerated Surface Area and Porosimetry Analyzer (Micromeritics Instrument Corporation, Norcross, GA) was used under nitrogen flow. Elemental analyses were carried out on a Therm Finnigan-CE Instruments, Flash EA 1112 CHNS series model. Thermogravimetric analysis (TGA) was carried out on a Thermal Analyser STA 449 F3 Jupiter at a heating rate of 5 °C min^{-1} in air atmosphere. Fourier transform infrared spectroscopy (FTIR) analysis measurements were carried out on a Bruker Tensor 27 (16 scans and 1 cm^{-1} resolution) at room temperature in the 4000 cm^{-1} to 400 cm^{-1} region. A small amount of each copolymer was mixed with dried KBr (1:5 mass ratio) and ground before recording. Electron paramagnetic resonance (EPR) spectroscopy was used to determine if radical species had been formed on the surface of the silica samples functionalized using plasma technology. The X-band EPR (9.66 GHz) spectra were recorded at room temperature (295 K) using a Bruker EMX 6/1 spectrometer and an ER4116DM rectangular cavity (Bruker). The acquisition conditions were a modulation frequency of 100 kHz, modulation amplitude of 0.05 mT and a microwave power of 6.36 mW. The approximate concentration of paramagnetic species was determined from the area beneath the integrated spectrum (double integration of the spectrum), using a 2,2,6,6-tetra-methyl-piperidin-nitroxide (TEMPO) solution in methanol as standard.

Gravity-driven column experiments

The binding capacity Q (mmol g^{-1}) was calculated by the following Eq. (1)

$$Q = \frac{(C_0 - C).V}{W} \quad (1)$$

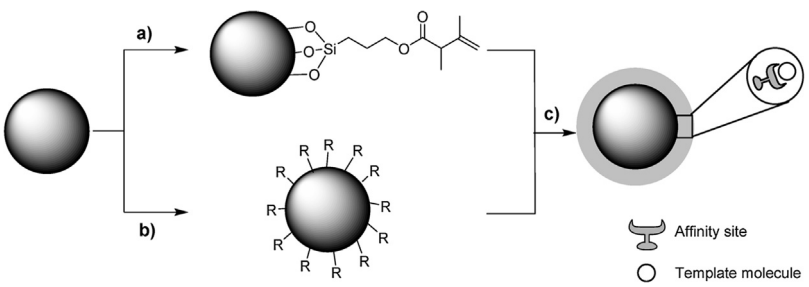

Fig. 2. General scheme to produce MIP-layered silica beads: (a) MPS-functionalization silica beads in $scCO_2$, (b) Plasma functionalization of silica beads, and (c) MIP-layered silica beads produced in $scCO_2$.

where C_0 and C were the template concentrations (mg mL^{-1}) in the solutions which were measured initially and after sorption, respectively; V was the volume of the solution and W (g) was the sample weight. In a typical experiment, 396.5 mg of core–shell MIP beads were packed on a gravity-fed blank column with a filter of 0.2 μm on the base (diameter: 1 cm, bed height: 1.5 cm). The column was operated in a gravitational mode, with no need to apply pressure or vacuum. Before its use, the column was conditioned with 10 mL of ACN. Then, 10 mL of solution containing 0.25 mg mL^{-1} of ACET, BENZ, PIV and a solution containing ACET and API (0.25 and 3.5 mg mL^{-1}) were passed through the MIP gravity-driven cartridge. Between each solution in this specific sequence, columns were washed exhaustively with 3 × 10 mL of ACN. Samples were analyzed by HPLC-UV using a method described as follows.

Chromatographic conditions

Chromatographic analyses of ACET, BENZ, PIV and API were carried out using a Dionex ICS-3000 with a Photo diode Array ICS series Dionex detector and Chromelleon Dionex v6.8. acer Veriton 6800 software. Experiments were carried out at 25 °C using a VertexPlus Column 250 × 4 mm Eurospher II 100-5 C18 with pre-column as stationary phase. UV detection was made at 220 nm. The isocratic mobile phase was used with a combination of aqueous buffered containing TFA at pH 2.5 and acetonitrile in the ratio 30:70% (v/v). A constant flow rate of 0.6 mL min^{-1} was employed throughout the analysis using a loop volume of 25 μL. The solvents used were filtrated with a 0.20 μm filter and degassed.

Results and discussion

The scheme shown in Fig. 2 depicts the synthetic procedure to obtain core–shell MIP beads which involves two different functionalization methods, the use of $scCO_2$ and plasma technology to produce a layer of MIP deposited on the surface of core–shell beads.

Core–shell MIP beads as stationary phase were designed using green methodologies specifically for use in gravity-driven processes. In this regard Fig. 2 shows schematically two different approaches to functionalize silica core–shell particles, *grafting to* and *grafting from* using MPS/EtOH-$scCO_2$ and plasma technology.

Fig. 3 shows SEM photographs of bare silica support and MIP-layered silica. The coverage of the silica surface by the imprinted polymer on Si-MPS-MIP is clearly visible, which is consistent with successful chemical grafting using MPS coupling agent as well as plasma functionalization. Also, in the case of Si-MPS-MIPs the thickness of the layer could be determine and varied from 122 to 453 nm as measured from the SEM image (Fig. 3).

Notably, the individual integrity of the particles was maintained when particles were functionalized using the different approaches. A thin MIP layer was grafted from the silica surface in Si-Plasma-E1 and Si-Plasma-E2. From the appearance of the particles it can be seen that different treatments generate different types of layers, signifying that the type of deposition used to produce the MIP surface layer plays an important role in adhesion of polymer to surface.

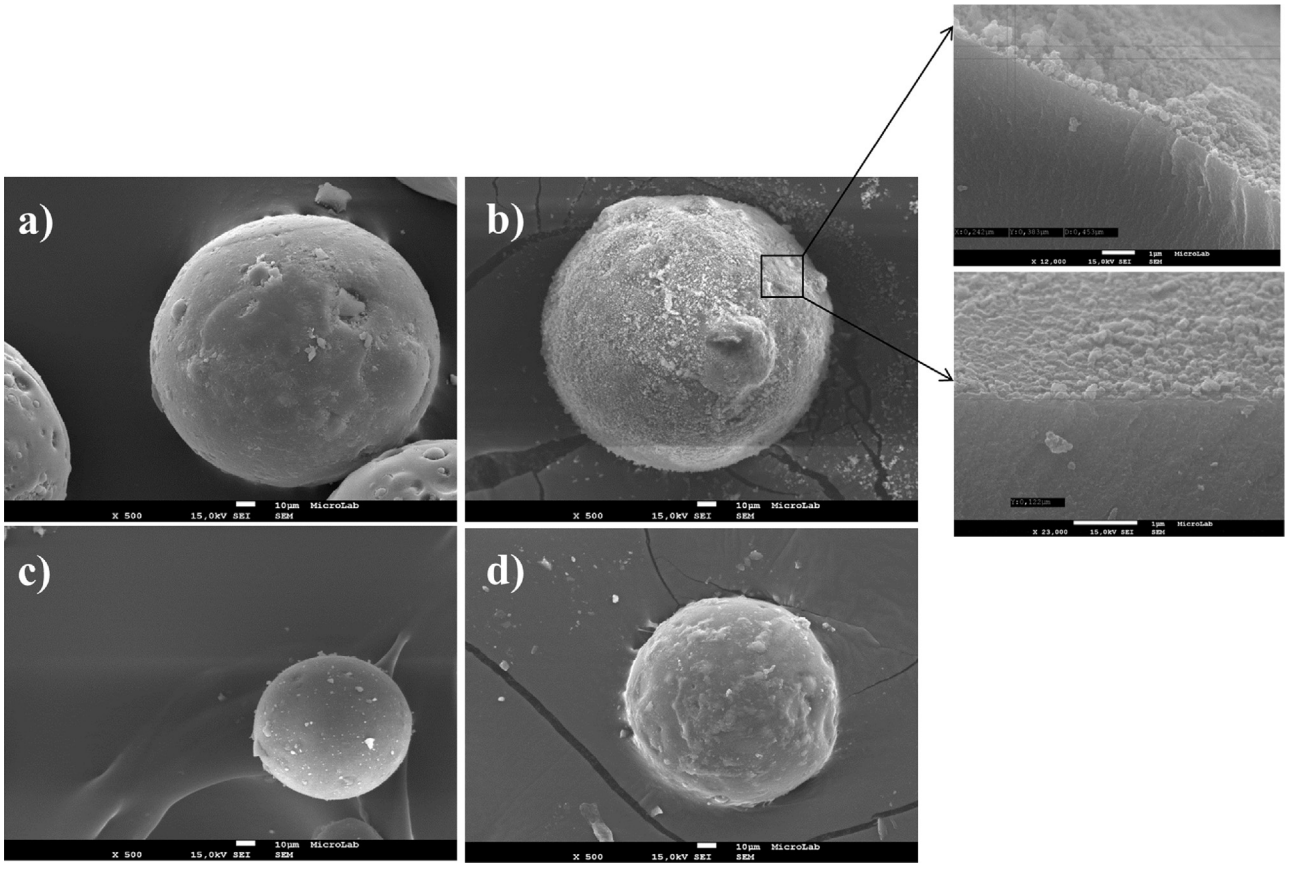

Fig. 3. SEM images obtained for: (a) silica beads; (b) Si-MPS-MIP and thickness measurements; (c) Si-Plasma-E1-MIP and (d) Si-Plasma-E2-MIP.

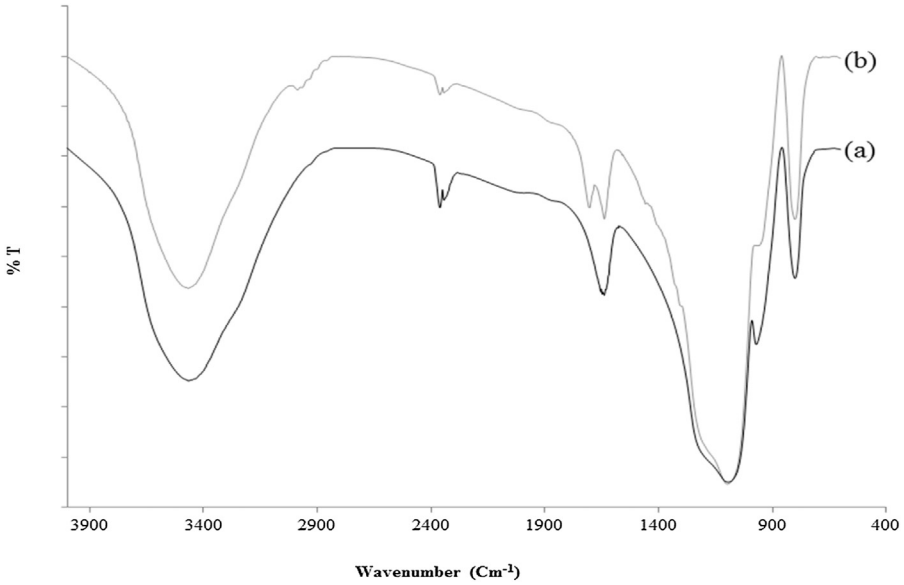

Fig. 4. FTIR analysis of: (a) Silica and (b) MPS functionalization of silica.

MPS/EtOH- $scCO_2$ functionalization

Herein, is the first reported functionalization of silica using MPS/EtOH employing $scCO_2$ technology. FTIR analysis (see Fig. 4) shows the characteristic peak at 1704 cm^{-1} (C=O) which prove the success of the functionalization step by "*grafting to*" method, as well as the characteristic peaks for silica: 1096 cm^{-1} —Si—O—Si; 3467 cm^{-1} – hydroxyl group on the surface; 1638 cm^{-1} —SiO—H bending; 970 cm^{-1}, 800 cm^{-1} – water in the sample; 1100 cm^{-1} —Si—O—C group; 1704 cm^{-1} - CH_3 and C=O groups.

Silica, functionalized silica particles (Si-MPS and Si-Plasma) and MIP coated silica particles were analyzed by nitrogen porosimetry. Multipoint BET method results (type II), shown in Table 1, evidences some differences between silica and functionalized silica regarding surface area, total pore volume and pore diameter. Silica particles have higher surface area and porosity, however after the functionalization step produced by MPS and Plasma they suffer a decrease in BET surface area, total pore volume and pore diameter establishing that there was an effective modification at silica surface. Additionally, MPS-functionalization led to a more significant decrease of these properties than Plasma functionalization and which probably strongly influences the coating of the MIP layer.

Elemental analysis and thermal stability were performed on all samples in order to understand the effect that the MPS surface modification had on the silica particles.

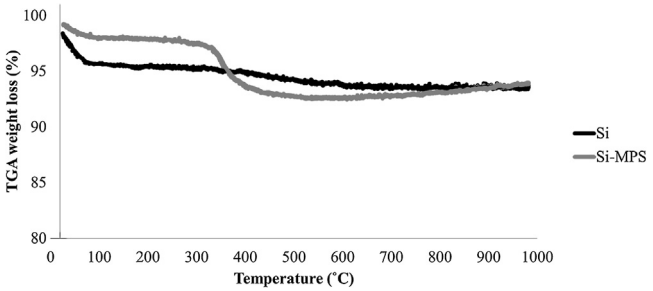

Fig. 5. TGA of silica and Si-MPS.

Fig. 5 shows the thermograms obtained for silica and Si-MPS samples. In both thermograms, there are a first weight loss until around 100 °C which can be attributed to the loss of water [40]. Between 350 °C and 450 °C there is a higher loss in Si-MPS (2.88%) which can be attributed to the presence of bound MPS, than for Si (0.42%) which practically remains the same, corresponding to an overall weight loss of 3.8% for Si particles and 6.2% for Si-MPS (*vide* Table 2).

MPS content on MPS-modified silica particles were quantified by equations based on elemental analysis and thermogravimetric analysis which are two methods for the determination of the silane

Table 1
Physical characteristics (surface area, average pore diameter and specific pore volume) of silica, Si-MPS-MIPs and Si-Plasma-MIPs obtained for all functionalization of silica by multipoint BET method (type II).

	BET surface area ($m^2 g^{-1}$)	Total pore volume ($cm^3 g^{-1}$)	Pore diameter (Å)
Si	385.5	0.99	67.3
Si-MPS	276.5	0.58	48.6
Si-MPS-NIP	222.3	0.17	36.0
Si-MPS-MIP	261.6	0.23	36.4
Si-Plasma-E1-NIP	329.6	0.84	66.0
Si-Plasma-E1-MIP	339.2	0.85	65.2
Si-Plasma-E2-NIP	291.3	0.74	65.0
Si-Plasma-E2-MIP	283.9	0.73	66.4

Table 2
Results obtained by elemental analysis and TGA as well as grafting density obtained by theoretical equations [9,10] for MPS/EtOH-functionalized silica in $scCO_2$.

	[MPS](μmol m^{-2})	Elemental analysis				TGA		
		%C	%H	Grafting density (μmol m^{-2})	Grafting yield (%)	Weight loss(%)	Grafting density (μmol m^{-2})	Grafting yield (%)
Si			0.68			3.8		
Si-MPS	12.64	9.32	1.54	2.49	19.72	6.2	0.293	2.32

coverage of silica surface. First, the silane grafting density was determined by elemental analysis from the carbon content using the Berendsen equation (Eq. (2))[41]

$$grafting\ density(\mu mol{\cdot}m^{-2}) = \frac{\Delta C}{[100.M_C.N_C - \Delta C(M_{MPS} - 1)]{\cdot}S} \times 10^6 \quad (2)$$

where ΔC is the difference between of carbon content (wt%) the sample and silica, M_C and N_C are the atomic mass (M_C = 12 g mol^{-1}) and the number of the carbon atoms of the grafted silane (N_C = 8), respectively. M_{MPS} is the molecular weight of the MPS silane (M_{MPS} = 248.35 g mol^{-1}) and S is the specific area of the silica (S = 385.5 m^2 g^{-1}). The grafting density was also determined by thermogravimetric analysis using Eq. (3) [42].

$$grafting\ density(\mu mol{\cdot}m^{-2}) = \frac{\left(\frac{W_{20-1000}}{100-W_{20-1000}}\right){\cdot}100 - W_{Silica}}{M_{MPS}{\cdot}S{\cdot}100} \times 10^6 \quad (3)$$

where $W_{20-1000}$ is the weight loss from 20 to 1000 °C, related to the degradation of the MPS and W_{Silica} is the weight loss of silica before grafting.

The TGA and elemental analysis was further used to calculate the grafting yield by the following Eq. (4),

$$grafting\ yield(\%) = \frac{grafting\ density}{[MPS]} \times 100 \quad (4)$$

where the concentration of MPS used, [MPS] (μmol m^{-2}) is calculated using the following Eq. (5),

$$[MPS] = \frac{W_{MPS}}{W_{Silica}{\cdot}S{\cdot}M_{MPS}} \quad (5)$$

where W_{MPS} and W_{Silica} are the weight of MPS and silica used in the reaction respectively. M_{MPS} is the molecular weight of MPS and S is the specific surface area of silica.

The results obtained for MPS grafting density by EA and TGA are listed in Table 2, respectively. Only MPS grafting can be compared with literature values reported by Pardal et al. [42] and Gupta et al. [43] although the values obtained by these authors for MPS grafting by elemental and thermogravimetric analysis are lower than the values obtained herein. These differences can be explained by considering other parameters such as particle size diameter and surface area of the particles, which in the literature cases, are nanoparticles with surface area equal to 200 m^2 g^{-1}. Another important difference is the fact that the previously published values are for the functionalization of silica particles using conventional methods, whilst in this work supercritical carbon dioxide was used to produce the modifications at the silica surface. In addition, literature reports indicate that the nature of the solvents also has a high influence on MPS grafting [41]. Functionalization of silica in supercritical medium has already been described in the literature but using silica nanoparticles and MEMO-silane coupling agent [44].

Grafting yields determined by elemental and thermogravimetric analysis are different—see Table 2, 19.72% and 2.32% respectively. In fact, it is difficult to compare these values obtained by EA and TGA because they are calculated using different assumptions.

Good results were achieved for grafting yields (Table 3) of MIP and NIP layers at the silica surface thus underscoring the use and potential of this green technology based on $scCO_2$ in comparison with traditional processes where grafting yields were very low [42,43].

Table 3
Results obtained by elemental analysis for Si-MPS-NIP and Si-MPS-MIP for determination of grafting density and grafting yield using theoretical equations [9,10].

Sample	Elemental analysis		
	% C	Grafting density (μmol m^{-2})	Grafting yield (%)
Si-MPS-NIP	21.22	14.06	100
Si-MPS-MIP	20.08	11.24	88.9

Plasma functionalization

Plasma technology was used to generate free radicals on the silica surface using two different conditions, **E1** (Ar) and **E2** (Ar + H_2), enabling the initiation of graft polymerization of an imprinted layer using a monomer and cross-linker, MAA and EGDMA respectively, *via* free radical process in $scCO_2$ solvent. The efficiency of the free radicals generated at the silica surface on the

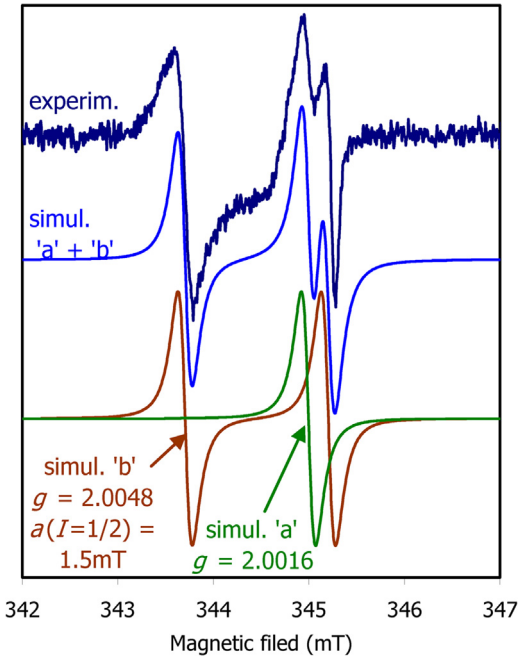

Fig. 6. EPR spectrum of Si-Plasma-E1. The experimental spectrum (dark blue line) was acquired at room temperature (295 K), with a microwave frequency of 9.66 GHz, modulation frequency of 100 kHz, modulation amplitude of 0.05 mT and a microwave power of 6.36 mW. The experimental spectrum can be simulated by the sum of two radical species (blue line), species 'a' (green line) plus species 'b' (brown line), with the EPR parameters indicated (For interpretation of the references to colour in this figure legend, the reader is referred to the web version of this article.).

grafting of the functional monomers is influenced by the nature and surface density of the free radical sites. These free radical sites can either be produced directly by the interaction of the plasma gas with the silica or result from secondary reactions involving the primary radicals [45].

The nature of the gas plasma had a significant impact on the silica functionalization which was reflected in the material's performance in the selective removal of ACET by the core–shell MIP beads.

The presence of radicals on silica functionalized by plasma technology was evaluated by EPR. The spectra of Si-Plasma-E1 and Si-Plasma-E2 were similar and showed that radical species were effectively produced at the silica surface. The EPR spectrum (Fig. 6) can be interpreted as arising from two radical species, 'a' and 'b', in which one species is under the influence of a hydrogen atom ($I = 1/2$) (for example, species 'a' with $g = 2.0016$ plus species 'b' with $g = 2.0048$ and a (H) = 1.5 mT, as is exemplified in the simulation presented in Fig. 6). Alternatively, the spectrum obtained could arise from three radical species, with g values of 2.0091, 2.0016 and 2.0004 (none under the influence of nuclei with a nuclear magnetic moment different from zero). The concentration of radical species presented on both samples, Si-Plasma-E1 and Si-Plasma-E2 was the same and could be determined from the simulated spectrum (Fig. 6, blue line), as described in *Experimental* section and found to be approximately 131 nM for both samples, corresponding to 1.23 pmol m^{-2}.

Elemental analysis for carbon content were 3.82% (Si-Plasma-E1-NIP), 0.55% (Si-Plasma-E1-MIP), 2.66% (Si-Plasma-E2-NIP) and 1.32% (Si-Plasma-E2-MIP). It is notable that carbon content of core–shell MIP beads produced using plasma technology was very low in comparison with MPS/EtOH-$scCO_2$ functionalization. This low value is obviously related to the amount of radicals that could be effectively introduced at the silica surface and the efficiency of these radicals in initiating the polymerization process under $scCO_2$.

Dynamic binding tests

The dynamic adsorption capacities of core–shell MIP and NIP beads for ACET was determined for a specific concentration of 0.25 mg mL^{-1} (see Fig. 7). In the case of core–shell particles functionalized using the MPS/EtOH procedure under $scCO_2$ it can be seen that Si-MPS-MIP adsorbs 1.3 times more ACET than Si-MPS-NIP, indicating that the imprinted device displayed a higher affinity to ACET than the non-imprinted device. Presumably the specific recognition cavities for ACET created at the surface of silica core–shell MIP beads retain the analyte via hydrogen bonds, as it has been reported that MAA is a monomer of choice to produce hydrogen bond donor–acceptor sites for ACET, potentially leading to sites with binary hydrogen bonds for this target impurity [46–50].

Si-Plasma-E2-MIPs presented the best performance in ACET capture, removing at least 48.76 μmol ACET per gram of support although the difference between the MIP and the NIP is relatively small. Si-Plasma-E2 both MIP and NIP have a better performance than the Si-Plasma-E1-MIP and NIP. Si-Plasma-E2-MIP had better performance, adsorbing more 19% than non-specific silica.

Selectivity measurements with analogue molecules

The selectivities were evaluated under competitive binding conditions using columns packed with untreated silica beads, MIPs and NIPs from the various grafting techniques using analogous

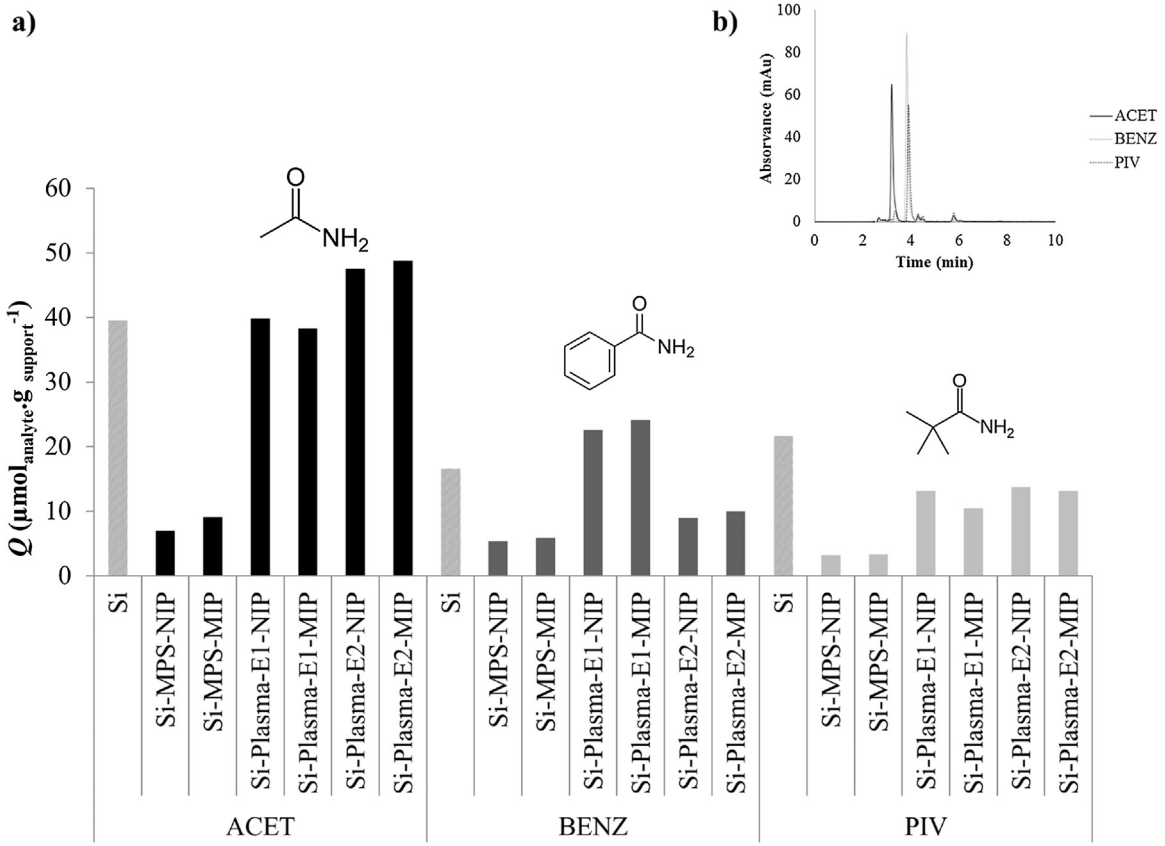

Fig. 7. (a) Binding and selectivity test on Si-MPS-MIPs, Si-Plasma-E1-MIPs and Si-Plasma-E2-MIPs with 0.25 mg mL^{-1} of each solution containing ACET, BENZ and PIV; (b) HPLC chromatograms of ACET, BENZ and PIV quantification.

molecules. BENZ and PIV were selected for this purpose due the similarity of their chemical structures to ACET and because they have different spatial requirements. Solutions containing 0.25 mg mL^{-1} of BENZ and PIV were passed though core–shell MIP columns. It can be seen from Fig. 7, that the affinity materials produced present higher adsorption capacity for ACET than BENZ or PIV.

Native silica core–shell beads captured higher amounts of ACET but it is well known that silica has no specific affinity and the surface adsorption is physical in nature [20,51]. ACET and API, which are very different chemical entities, both show a 5.7% adsorption capacity (see Fig. 9) is in line with this lack of specificity.

Gravity-driven column for API purification

Core–shell MIP beads were also evaluated as packing in gravity-driven columns for the removal of ACET from a mixture containing ACET and API as a model system for a real pharmaceutical situation. Firstly, 395.6 mg core–shell MIP beads were packed into commercially available empty columns (SPE tube—diameter: 1 cm, bed height: 1.5 cm) and washed several times with acetonitrile to equilibrate the stationary phase. Hereafter, the model mixture was loaded on columns and the fractions were collected for further analysis on HPLC. Fig. 8 shows a typical HPLC chromatogram.

As it can be seen from Fig. 9, the percentage of removal of ACET by Si-MPS-MIP was 38%, almost 10% more than Si-MPS-NIP. Contrary to expected, Si-MPS-MIP also absorbed more API than Si-MPS-NIP. Si-Plasma-E1 and Si-Plasma-E2 MIPs and NIPs removed higher amounts of ACET.

Higher adsorption of API was achieved by Si-Plasma-E2-MIP, around 30%, but Si-Plasma-E1-MIP only adsorbed 0.37% of API, whilst both removed 100% of ACET. The only difference in the preparation of E1 and E2 core beads is the use of different gases to generate plasma, argon and argon + hydrogen respectively. Hence, different types of surfaces having a strong influence on adsorption capacity are dependent on the gas system used in plasma formation.

Control beads, Si, were also evaluated for recognition and selectivity and were compared with Si-MPS and Si-Plasma based beads. As expected, bare silica beads did not show any specificity and adsorbed around 6% of both ACET and API, meaning that a physical adsorption process is taking place.

The Si-Plasma-E1-MIP removes totally ACET from the mixture with minimum loss of API (Fig. 9) thus showing high potential for pharmaceutical purification processes.

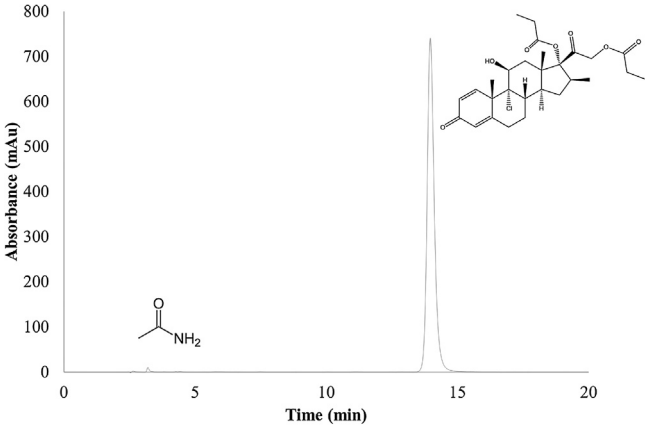

Fig. 8. HPLC chromatogram for selectivity test for Si-MPS-MIP, 25 μL of a model solution of ACET and API (0.25 mg mL^{-1} + 3.5 mg mL^{-1}).

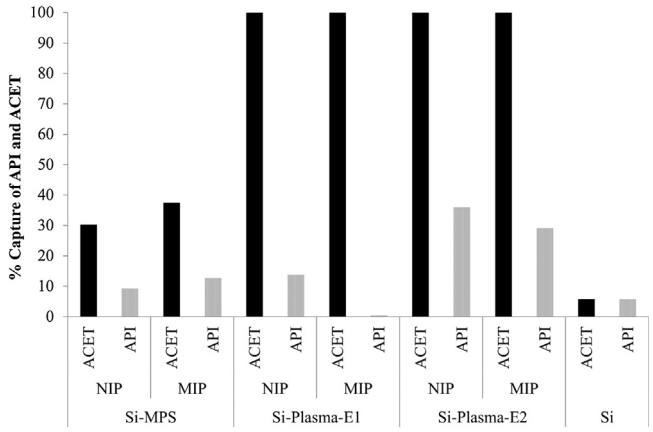

Fig. 9. Selective removal of ACET and API in percentage by core–shell MIP beads: 10 mL of a solution of ACET (0.25 mg mL^{-1}) and API (3.5 mg mL^{-1}) in ACN was loaded on 396.5 mg of core–shell MIPs and NIPs.

Szekely et al. [52] reported the synthesis and performance of molecularly imprinted microparticles (25–50 μm) for the removal of ACET when used as packing for a solid phase extraction column and applied to a solution containing ACET and an API (Etodolac). These MIP microparticles were able to remove 100% of ACET with 14% of API loss.

The methodology reported herein, uses a different approach employing Si-MPS-MIPs and Si-Plasma-E1-MIPs where lower losses of API were achieved: 12% (Si-MPS-MIPs) and 0.37% (Si-Plasma-E1-MIPs). While it representing a significant decrease in API loss, in particular, for the Si-Plasma-E1-MIPs, our core–shell MIP beads also can operate as column packing for gravity flow columns negating the need of applying pressure or vacuum, commonly used in solid-phase extraction apparatus and thus significantly reducing the costs associated.

Conclusions

The present article reports the functionalization of silica core–shell beads using *grafting to* and *grafting from* strategies using green technologies: MPS/EtOH-$scCO_2$ and plasma technology. Functionalization of silica core–shell beads was successfully achieved using these green technologies as confirmed by FTIR and EPR analysis. Furthermore, the MIP layers (using ACET, a model genotoxin, as template) were synthesized on pre-functionalized silica core–shell beads using $scCO_2$ technology with MAA as monomer and EGDMA as cross-linker. Core–shell beads were packed into columns and the selective removal of ACET was evaluated versus analogue molecules (BENZ and PIV) and with a model solution containing ACET and API. Si_Plasma_E1_MIPs showed to be able to remove 100% of ACET with a minimal loss of API (0.37%) revealing to be a promising packing to remove genotoxins from APIs in an industrial environment.

Acknowledgments

The authors would like to thank financial support from Fundação para a Ciência e Tecnologia/Ministério da Ciência, Tecnologia e Ensino Superior (FCT/MCTES), Portugal, through principal investigator contract IF/00915/2014 (T.C.), projects UID/QUI/50006/2013, UID/Multi/04378/2013, UID/FIS/50010/2013 and PTDC/QEQ-PRS/2757/2012. R.V. would like to thank FCT/MCTES and HOVIONE for her doctoral grant SFRH/BDE/51907/2012. Beclomethasone dipropionate, the API sample, was kindly provided by Hovione FarmaCiencia SA. This work was also supported by the Associate Laboratory Research Unit for Green

Chemistry – Clean Technologies and Processes – LAQV and Unidade de Ciências Biomoleculares Aplicadas – UCIBIO which are financed by national funds from FCT/MCTES (UID/QUI/50006/2013) and (UID/Multi/04378/2013) respectively co-financed by the ERDF under the PT2020 Partnership Agreement (POCI-01-0145-FEDER-007265) and (POCI-01-0145-FEDER-007728). L.B.M. thanks FCT/MCTES, for a fellowship grant (SFRH/BPD/111404/2015, which is financed by national funds and co-financed by FSE). We also would like to thank Professor Miguel Teixeira (ITQB, UNL, Portugal) for having facilitated the use of the EPR spectrometer. The authors would like to acknowledge Nuno Costa from REQUIMTE analytical services for his support in the development of HPLC methods for amides quantification.

References

[1] J. Pennington, R.D. Cohen, Y. Tian, F. Boulineau, J. Pharm. Biomed. Anal. 114 (2015) 488.
[2] Committee for Medicinal Products for Human Use (CHMP), Questions and answers on the Guideline on the limits of genotoxic impurities. European Medicines Agency. Available at: http://www.ema.europa.eu/docs/en_GB/document_library/Scientific_guideline/2009/09/WC500002907.pdf.
[3] J.F. Contrera, Regul. Toxicol. Pharmacol. 59 (2011) 133.
[4] W.E. Siew, A.G. Livingston, C. Ates, A. Merschaert, Sep. Purif. Technol. 102 (2013) 1.
[5] G. Székely, M. Gil, B. Sellergren, W. Heggie, F.C. Ferreira, Green Chem. 15 (2013) 210.
[6] M. Degerman, N. Jakobsson, B. Nilsson, Chem. Eng. Technol. 31 (2008) 875.
[7] European Medicines Agency, doc. ref. EMEA/CHMP/QWP/251334/2006.
[8] N.V.V.S.S. Raman, A.V.S.S. Prasad, K.R. Reddy, J. Pharm. Biomed. Anal. 55 (2011) 662.
[9] S.P. Raillard, Org. Process Res. Dev. 14 (2010) 946.
[10] G. Székely, J. Bandarra, W. Heggie, F.C. Ferreira, B. Sellergren, Sep. Purif. Technol. 86 (2012) 190.
[11] S.G. Del Blanco, L. Donato, E. Drioli, Sep. Purif. Technol. 87 (2012) 40.
[12] M. Shamsipur, J. Fasihi, K. Ashtari, Anal. Chem. 79 (2007) 7116.
[13] T.E. Milja, K.P. Prathish, T.P. Rao, J. Hazard. Mater. 188 (2011) 384.
[14] C. He, Y. Long, J. Pan, K. Li, F. Liu, J. Biochem. Biophys. Methods 70 (2007) 133.
[15] W. Zhao, N. Sheng, R. Zhu, F. Wei, Z. Cai, M. Zhai, S. Du, Q. Hu, J. Hazard. Mater. 179 (2010) 223.
[16] B. Yu, C. Tian, H. Cong, T. Xu, J. Mater. Sci. 51 (2016) 5240.
[17] C. Lu, H. Li, M. Xu, S. Wang, G. Li, W. Zhong, S. Qin, Sep. Sci. Technol. 50 (2015) 2124.
[18] J. Li, Z. Zhang, S. Xu, L. Chen, N. Zhou, H. Xiong, H. Peng, J. Mater. Chem. 21 (2011) 19267.
[19] D. Gao, Z. Zhang, M. Wu, C. Xie, G. Guan, D. Wang, J. Am. Chem. Soc. 129 (2007) 7859.
[20] R. Liu, G. Guan, S. Wang, Z. Zhang, Analyst 136 (2011) 184.
[21] V.G. Ngo, C. Bressy, C. Leroux, A. Margaillan, Polymer 50 (2009) 3095.
[22] M.L. Hair, D. Guzonas, D. Boils, Macromolecules 3 (1991) 341.
[23] L. Han, Z. Mao, J. Wu, Y. Guo, T. Ren, C. Gao, Biomaterials 34 (2013) 975.
[24] S. Hansson, V. Trouillet, T. Tischer, A.S. Goldmann, A. Carlmark, C. Barner-Kowollik, E. Malmström, Biomacromolecules 14 (2013) 64.
[25] J.S. Basuki, L. Esser, P.B. Zetterlund, M.R. Whittaker, C. Boyer, T.P. Davis, Macromolecules 46 (2013) 6038.
[26] T. Barroso, R. Viveiros, M. Temtem, T. Casimiro, A.M. Botelho Do Rego, A. Aguiar-Ricardo, ACS Macro Lett. 1 (2012) 356.
[27] M. Soares da Silva, F.L. Nobrega, A. Aguiar-Ricardo, E.J. Cabrita, T. Casimiro, J. Supercrit. Fluids 58 (2011) 150.
[28] M. Soares da Silva, R. Viveiros, M.B. Coelho, A. Aguiar-Ricardo, T. Casimiro, Chem. Eng. Sci. 68 (2012) 94.
[29] A.N.C. Martins, S.P. Simeonov, L.M.T. Frija, R. Viveiros, A. Lourenço, M. Soares da Silva, T. Casimiro, C.A.M. Afonso, Ind. Crops Prod. 60 (2014) 226.
[30] E.J. Park, W.S. Kim, H.S. Hwang, C. Park, K.T. Lim, Macromol. Symp. 249–250 (2007) 196.
[31] D. Stojanovic, A. Orlovic, S. Markovic, V. Radmilovic, P.S. Uskokovic, R. Aleksic, J. Mater. Sci. 44 (2009) 6223.
[32] B.B. Prasad, S. Banerjee, React. Funct. Polym. 55 (2003) 159.
[33] B.B. Prasad, S. Banerjee, Chromatographia 55 (2002) 171.
[34] U. Reddy, M.K. Hussain, V. Bobbarala, S. Penumajji, Int. J. Pharm. Bio Sci. 2 (2011) 453.
[35] G. Huchon, H. Magnussen, A. Chuchalin, L. Dymek, F.B. Gonod, J. Bousquet, Respir. Med. 103 (2009) 41.
[36] E.O. Meltzer, R.L. Jacobs, C.F. LaForce, C.L. Kelley, S.A. Dunbar, S.K. Tantry, Allergy Asthma Proc. 33 (2012) 249.
[37] M. Moisan, Z. Zakrzewski, J. Phys. D. Appl. Phys. 24 (1991) 1025.
[38] E. Tatarova, A. Dias, J. Henriques, A.M. Botelho do Rego, A.M. Ferraria, M.V. Abrashev, C.C. Luhrs, J. Phillips, F.M. Dias, C.M. Ferreira, J. Phys. D Appl. Phys. (2014) 385501.
[39] T. Casimiro, A.M. Banet-Osuna, A.M. Ramos, M. Nunes da Ponte, A. Aguiar-Ricardo, Eur. Polym. J. 41 (2005) 1947.
[40] I. Freris, D. Cristofori, P. Riello, A. Benedetti, J. Colloid Interface Sci. 331 (2009) 351.
[41] E. Bourgeat-Lami, P. Espiard, A. Guyot, Polymer 36 (1995) 4385.
[42] F. Pardal, V. Lapinte, J.J. Robin, J. Polym. Sci. Part A Polym. Chem. 47 (2009) 4617.
[43] S. Gupta, P.C. Ramamurthy, G. Madras, Polym. Chem. 2 (2011) 221.
[44] D. Stojanovic, A. Orlovic, S.B. Glisic, S. Markovic, V. Radmilovic, P.S. Uskokovic, R. Aleksic, J. Supercrit. Fluids 52 (2010) 276.
[45] L. Andreozzi, V. Castelvetro, G. Ciardelli, L. Corsi, M. Faetti, E. Fatarella, F. Zulli, J. Colloid Interface Sci. 289 (2005) 455.
[46] M. Syu, J. Deng, Y. Nian, Anal. Chim. Acta 504 (2004) 167.
[47] H.Y. Wang, S.L. Xia, H. Sun, Y.K. Liu, S.K. Cao, T. Kobayashi, J. Chromatogr. B Anal. Technol. Biomed. Life Sci. 804 (2004) 127.
[48] F. Chapuis, V. Pichon, F. Lanza, B. Sellergren, M.-C. Hennion, J. Chromatogr. B 804 (2004) 93.
[49] J. Jodlbauer, N.M. Maier, W. Lindner, J. Chromatogr. A 945 (2002) 45.
[50] P.T. Vallano, V.T. Remcho, J. Chromatogr. A 888 (2000) 87.
[51] R. Zhu, W. Zhao, M. Zhai, F. Wei, Z. Cai, N. Sheng, Q. Hu, Anal. Chim. Acta 658 (2010) 209.
[52] G. Székely, E. Fritz, J. Bandarra, W. Heggie, B. Sellergren, J. Chromatogr. A 1240 (2012) 52.